Human Genetics (2019) 138:1247–1257
https://doi.org/10.1007/s00439-019-02063-z

ORIGINAL INVESTIGATION

MDH1 deficiency is a metabolic disorder of the malate–aspartate shuttle associated with early onset severe encephalopathy

Melissa H. Broeks[1] · Hanan E. Shamseldin[2] · Amal Alhashem[3] · Mais Hashem[2] · Firdous Abdulwahab[2] · Tarfa Alshedi[2] · Iman Alobaid[2] · Fried Zwartkruis[4] · Denise Westland[1] · Sabine Fuchs[5] · Nanda M. Verhoeven-Duif[1] · Judith J. M. Jans[1] · Fowzan S. Alkuraya[2]

Received: 12 July 2019 / Accepted: 9 September 2019 / Published online: 19 September 2019

Abstract

The reversible oxidation of L-malate to oxaloacetate is catalyzed by NAD(H)-dependent malate dehydrogenase (MDH). MDH plays essential roles in the malate–aspartate shuttle and the tricarboxylic acid cycle. These metabolic processes are important in mitochondrial NADH supply for oxidative phosphorylation. Recently, bi-allelic mutations in mitochondrial MDH2 were identified in patients with global developmental delay, epilepsy and lactic acidosis. We now report two patients from an extended consanguineous family with a deleterious variant in the cytosolic isoenzyme of MDH (MDH1). The homozygous missense variant in the NAD^+-binding domain of MDH1 led to severely diminished MDH protein expression. The patients presented with global developmental delay, epilepsy and progressive microcephaly. Both patients had normal concentrations of plasma amino acids, acylcarnitines, lactate, and urine organic acids. To identify the metabolic consequences of MDH1 deficiency, untargeted metabolomics was performed on dried blood spots (DBS) from the patients and in MDH1 knockout HEK293 cells that were generated by Crispr/Cas9. Increased levels of glutamate and glycerol-3-phosphate were found in DBS of both patients. In MDH1 KO HEK293 cells, increased levels of glycerol-3-phosphate were also observed, as well as increased levels of aspartate and decreased levels of fumarate. The consistent finding of increased concentrations of glycerol-3-phosphate may represent a compensatory mechanism to enhance cytosolic oxidation of NADH by the glycerol-*P*-shuttle. In conclusion, MDH1 deficiency is a new metabolic defect in the malate–aspartate shuttle characterized by a severe neurodevelopmental phenotype with elevated concentrations of glycerol-3-phosphate as a potential biomarker.

Abbreviations

MDH	Malate dehydrogenase
MAS	Malate–aspartate shuttle
TCA	Tricarboxylic acid
DBS	Dried blood spot
LC–MS/MS	Liquid chromatography–mass spectrometry and tandem mass spectrometry
Glycerol-3-*P*	Glycerol 3-phosphate
Glycerol-*P*	Glycerol phosphate

Melissa H. Broeks and Hanan E. Shamseldin have contributed equally to this work.

Electronic supplementary material The online version of this article (https://doi.org/10.1007/s00439-019-02063-z) contains supplementary material, which is available to authorized users.

✉ Judith J. M. Jans
J.J.M.Jans@umcutrecht.nl

✉ Fowzan S. Alkuraya
falkuraya@kfshrc.edu.sa

[1] Section Metabolic Diagnostics, Department of Genetics, University Medical Center Utrecht, 3584 EA Utrecht, The Netherlands

[2] Department of Genetics, King Faisal Specialist Hospital and Research Center, Riyadh 12713, Saudi Arabia

[3] Department of Pediatrics, Prince Sultan Military Medical City, Riyadh 11159, Saudi Arabia

[4] Department of Molecular Cancer Research, Center for Molecular Medicine, University Medical Center Utrecht, 3584 CX Utrecht, The Netherlands

[5] Section Metabolic Diseases, Department of Child Health, Wilhelmina Children's Hospital, University Medical Center Utrecht, 3584 EA Utrecht, The Netherlands

Introduction

Malate dehydrogenase 1 (MDH1), an NAD(H)-dependent enzyme, is a part of the malate–aspartate shuttle (MAS). MAS is important for intracellular NAD(H) redox homeostasis as it transfers reducing equivalents across the mitochondrial membrane. NAD(H) itself cannot pass the mitochondrial inner membrane (Fig. 1). Cytosolic and mitochondrial NAD^+/NADH pools are independent from each other, and a proper balance of redox state per compartment is important for cell proliferation and cell growth (Hanse et al. 2017; Olguín-Albuerne and Morán 2018). A constant supply of cytosolic NAD^+ is required to sustain

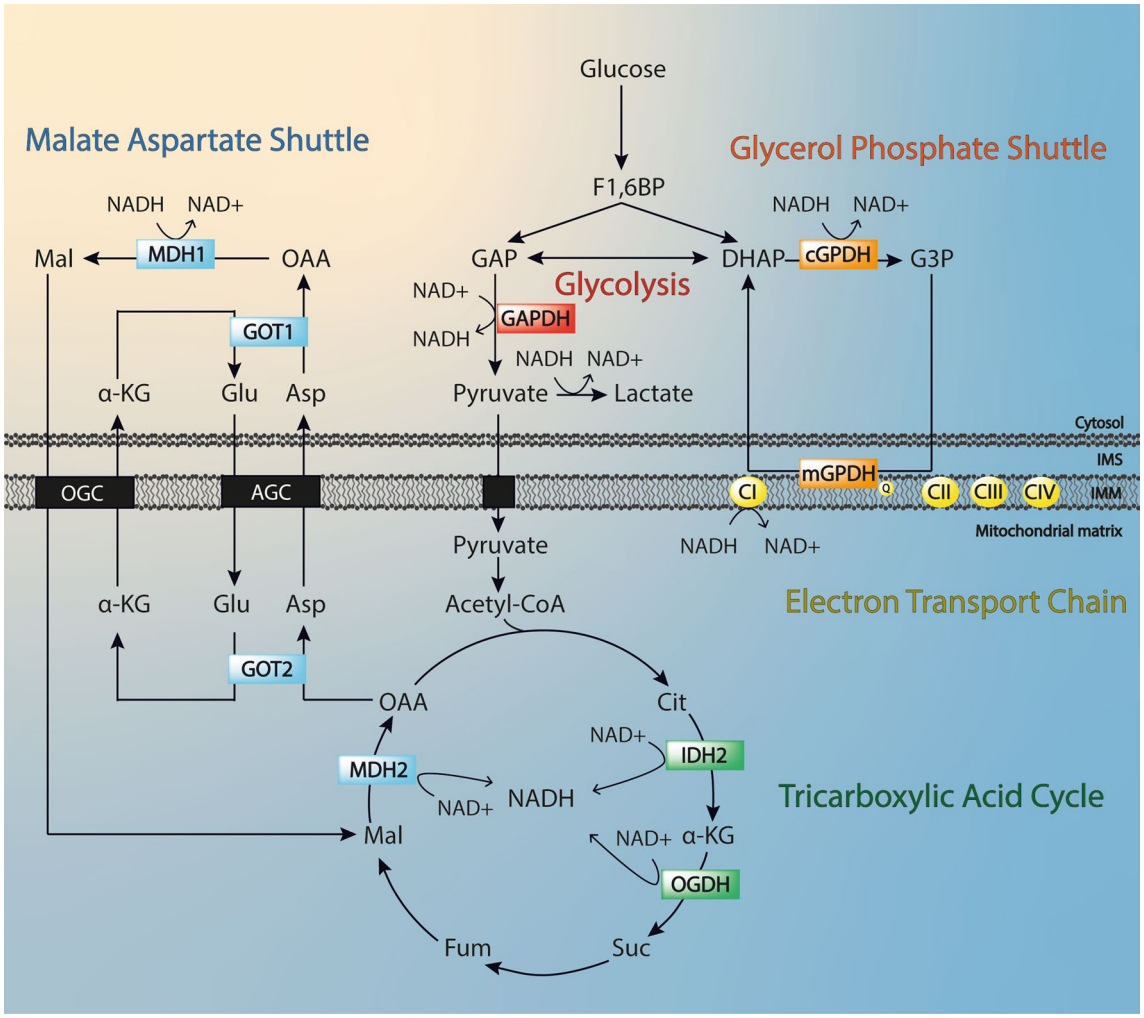

Fig. 1 Schematic overview of oxidative glucose metabolism and NAD(H) redox shuttles. NADH generated in the cytosol needs to be shuttled across the mitochondrial membrane, using NAD(H) redox shuttles. During glycolysis, fructose-1,6-bisphosphate (F1,6BP) is converted into glyceraldehyde-3-phosphate (GAP) and dihydroxyacetone phosphate (DHAP). The lower part of glycolysis converts GAP into pyruvate, generating NADH via glyceraldehyde-3-phosphate dehydrogenase (GAPDH). Cytosolic NADH is mainly shuttled into mitochondria via the malate aspartate shuttle, which requires the action of cytosolic and mitochondrial malate dehydrogenase (MDH1 and MDH2). Other components are cytosolic and mitochondrial glutamate aspartate transaminase (GOT1 and GOT2), the mitochondrial aspartate–glutamate carriers (AGC1 and AGC2), and the malate-oxoglutarate carrier (OGC). Pyruvate is converted into acetyl-CoA, which then enters the tricarboxylic acid cycle. The tricarboxylic acid cycle generates NADH from isocitrate dehydrogenase (IDH2), oxoglutarate dehydrogenase (OGDH), and also includes MDH2. Electrons of these mitochondrial NADH dehydrogenases enter the electron transport chain at the level of complex I (CI). In the glycerol phosphate shuttle, DHAP from glycolysis is further reduced to glycerol 3-phosphate (G3P) by cytosolic G3P dehydrogenase (cGPDH). Electrons from the reconversion to DHAP by mitochondrial GPDH enter the electron transport chain at the level of the quinol pool (Q). *Mal* malate, *OAA* oxaloacetate, *a-KG* alpha-ketoglutarate, *Glu* glutamate, *Asp* aspartate, *Cit* citrate, *Suc* succinate, *Fum* fumarate, *CII* complex II (succinate dehydrogenase), *CII* complex III, *CIV* complex IV, *NADH* nicotinamide adenine dinucleotide (reduced form), *NAD+*, nicotinamide adenine dinucleotide (oxidized form), *IMS* intermembrane space, *IMM* inner mitochondrial membrane

glycolysis via glyceraldehyde-3-phosphate dehydrogenase (Hanse et al. 2017). Replenishing cytosolic NAD^+ occurs via the reversible reduction of oxaloacetate to L-malate by MDH1 (Webb et al. 1973). Oxidation of L-malate to oxaloacetate by MDH2 occurs in mitochondria as part of both the MAS and tricarboxylic acid (TCA) cycle. This reaction generates NADH for the electron transport chain. The two MDH isoenzymes act in conjunction with four additional components: the cytosolic and the mitochondrial aspartate aminotransferases, and two mitochondrial carriers: the malate–oxoglutarate carrier and the aspartate–glutamate carrier (AGC). The latter exists in two isoforms that are expressed in a tissue-specific manner; AGC1 is mainly expressed in the brain and AGC2 in the liver (Palmieri et al. 2001).

Although both MDH enzymes have a high degree of three-dimensional structure conservation, they share a sequence-level homology of only ~ 20–25% and display different kinetics (Birktoft et al. 1989; Joh et al. 1987). Expression of MDH1 correlates with high aerobic metabolic demands in a tissue-specific manner. The most abundant expression is in the heart, skeletal muscle and brain, and to a lesser extent in smooth muscle and kidney, with low expression in the liver (Joh et al. 1987; Tanaka et al. 1996; Lo et al. 2005). MDH2 has a similar tissue-specific expression pattern as MDH1, which is consistent with the fact that they work co-operatively in the MAS to transport NADH across the mitochondrial membrane (Lo et al. 2005).

Since malate dehydrogenase plays a central role in metabolism via the MAS and the TCA cycle, it is a well-studied enzyme. Senescence is associated with decreased MDH1 activity (Lee et al. 2012). Conversely, MDH1 depletion has been shown to induce senescence (Lee et al. 2012). The role of MDH1 in the nucleus has been studied less. Upon glucose deprivation, MDH1 facilitates the binding of p53 to the promotor of downstream genes (Lee et al. 2009). Other studies of MDH1 in the context of human diseases have been limited to oncology. It has been noted that MDH1 activity correlates with the malignant potential of certain cancers, e.g., lung (Zhang et al. 2017). This is thought to be mediated by glycolytic-related ATP production.

No human disease-causing mutations in MDH1 have been reported to date; however, genetic diseases in the four other MAS components are known. The first disease reported was associated with mutations in *AGC2* (or *SLC25A13*). Patients presented with hyperammonemia and hepatic encephalopathy-like symptoms (OMIM #603471, #605814) (Saheki and Kobayashi 2002; Song et al. 2011). Subsequently, *AGC1* (or *SLC25A12*) deficiency was described in patients presenting with global developmental delay, encephalopathy and hypotonia (OMIM #612949) (Wibom et al. 2009; Falk et al. 2014). A deficiency in the mitochondrial aspartate aminotransferase *GOT2* leads to a similar phenotype as *AGC1* deficiency, with additional hyperammonemia and lactic acidosis (van Karnebeek et al. 2019). The fourth defect was recently discovered in *MDH2*. This defect is also characterized by global developmental delay, epilepsy and lactic acidosis (OMIM #617339) (Ait-El-Mkadem et al. 2017). Here, we report a deficiency in *MDH1* as the fifth MAS defect. Two patients from an extended consanguineous family were identified with a pathogenic homozygous *MDH1* variant. They both presented with a neurological phenotype that includes global developmental delay, epilepsy and progressive microcephaly.

Materials and methods

Human subjects

Patients, parents and other available relatives were recruited under an IRB-approved research protocol (KFSRHC RAC# 2080006) with informed consent. Venous blood was collected in EDTA tubes for DNA extraction and sodium heparin tubes for LCL establishment. A skin biopsy was also obtained from one patient for fibroblast culture. Bloodspots from both patients and three healthy controls were collected on a Guthrie card filter paper blood spot card and shipped from Saudi Arabia to the Netherlands. Dried bloodspots (DBS) were stored at − 80 °C until analysis in a zip lock bag containing a silica gel bag.

Cell culture, protein extraction and western blot of affected cells

Affected and control fibroblasts and Lymphoblastoid cell lines (LCL) were cultured in Minimum Essential Medium Eagle (Sigma-Aldrich M-5650) and RPMI (Thermo Fisher Scientific, 22400-089) media, respectively. Both media were supplemented with 15% v/v heat-inactivated fetal bovine serum (Thermo Fisher Scientific, cat No. 16140071), 1% v/v L-glutamine, and 1% v/v penicillin and streptomycin. Both cell types were cultured in a humidified, 5% CO_2 atmosphere at 37 °C. Protein extraction for western blot of patient cell lines was performed using RIPA buffer (Sigma-Aldrich, Cat. No. R0278) and protease inhibitor (Thermo Fisher Scientific, Cat No. 78438). Western blot was performed on affected and control protein extracts using a rabbit anti-MDH1 polyclonal antibody (Thermo Fisher Scientific, Cat. No. PA5-50446; diluted 1:1000). A mouse anti-alpha Tubulin monoclonal antibody (Abcam Cat. No. ab7291; diluted 1:1000) was used as loading control.

Generation of MDH1-knockout Hek293T cells by CRISPR-Cas9

Hek293T cells were transiently transfected with pSpCas9(BB)-2A-GFP (PX458), encoding a sgRNA targeting *MDH1* (sgRNA1 : ATTTATCTAAGGCTGCACCC, or sgRNA2: CTTCTTGGCGTATTTATCTA). GFP-positive cells were sorted using a FACSAria II flow cytometer (BD) and plated in 10-cm dishes. Colonies were picked from these plates after 1 week and checked for the absence of MDH1 by Western blot analysis using a mouse anti-MDHC (H6) monoclonal antibody (Santa Cruz cat. sc-166879; diluted 1:5000). A mouse anti-β-Catenin monoclonal antibody (BD Biosciences Cat. 610154; diluted 1:5000) was used as loading control.

Cell culture of Hek293T cells

Dulbecco's Modified Eagle Medium (DMEM), high glucose, GlutaMAX™, pyruvate (Cat. No. 31966); fetal bovine serum (FBS; Cat. No. 10270); penicillin–streptomycin (P/S (10,000 U/ml); Cat. No. 15140) and trypsin–ethylenediaminetetraacetic acid (trypsin–EDTA (0.5%), no phenol red; Cat. No. 15400) were purchased from Gibco™ (ThermoFisher Scientific).

Hek293T cells were cultured in 75 cm^2 filter cap flasks in a humidified, 5% CO_2 atmosphere at 37 °C. They were cultured in DMEM, high glucose, GlutaMAX™, pyruvate (with 10% (v/v) heat-inactivated FBS and 1% P/S (v/v)). Cells were passaged upon reaching confluence and medium was refreshed every 48 h.

Collection of cell lysates for metabolomics

MDH1 WT and KO HEK293 cells were plated in 6-well plates and cultured until full confluency. Medium was refreshed 24 after plating and 24 h before cell collection. Cell collection was done by washing cells with cold PBS (4 °C), followed by cell scraping in 1 ml ice-cold methanol. Next, methanol samples were transferred into 1.5-ml Eppendorf tubes, centrifuged (16,200*g* for 10 min at 4 °C), and then supernatants were transferred to new 1.5-ml Eppendorf tubes. The samples were evaporated at 40 °C under a gentle stream of nitrogen until complete dryness, and reconstituted with 500 µl of UPLC-grade methanol (room temperature). The reconstituted samples were stored at − 80 °C until analysis was performed.

Targeted metabolomics by LC–MS/MS

Amino acids

To quantify amino acids in DBS and cell lysates, we adapted the UPLC–MS/MS method that was previously described (Prinsen et al. 2016). The range of calibrators was adapted to our samples' concentrations. Furthermore, quality control samples that resembled the concentrations of our samples were used. No further adaptations were needed for sample preparation or analysis of the amino acids. The assay was performed in biological triplicates and data were corrected for total protein concentration.

TCA cycle intermediates

The quantification of TCA cycle intermediates in cell lysates was performed on a WatersAcquity ultraperformance liquid chromatography system (Waters Corp., Milford, USA). Chromatographic separation was performed at 30 °C using an Acquity HSS T3 column (100 mm × 2.1 mm i.d., 1.8 µm; Waters Corp.) equipped with an ACQUITY UPLC VanGuard Pre-Column HSS T3 (5 mm × 2.1 i.d., 1.8 µm). Two eluents were used. Solvent A contained 0.1% formic acid (v/v) dissolved in water provided by a Millipore system; solvent B contained 100% acetonitrile. The gradient elution was as follows: 0–4.0 min isocratic 1% B, 4.0–4.5 min linear from 1 to 100% B, 4.5–5.0 min isocratic 100% B, and 5.0–5.1 min linear from 100 to 1% B, with 5.1–6.0 min for initial conditions of 1% B for column equilibration. The flow rate remained constant at 0.3 ml/min. Injection volume was 10 µl.

Calibration standards were prepared with internal standards in the concentration range of 0.05–100 µM. Internal standards were added to 500 µl of cell extract, evaporated with nitrogen and reconstituted in 50 µl of eluent solvent A. UPLC/MS-grade methanol, formate, citrate, isocitrate, fumarate, pyruvate, succinate, lactate, malate, a-ketoglutarate and the internal standards $^{13}C_2$-succinate and $^{13}C_3$-lactate were obtained from Sigma-Aldrich, Denmark.

Detection of the metabolites was performed using a Waters Xevo triple quadrupole tandem mass spectrometer (Waters Corp., Manchester, UK) with a Z-spray electrospray ionization (ESI) source operating both in the positive and negative ion modes. The mass spectrometer was tuned for each individual metabolite to obtain the maximum intensity for the precursor ions. Parameters for ESI–MS analysis in negative ion/positive ion mode were as follows: capillary (kV) 2.5/3.0, extractor (V) 3/3, LM1 (low mass)/HM1 (high mass) resolution 3.0/15.0 and LM2/HM2 resolution 3.0/15.0. Desolvation gas flow rate was 800 l/h at a temperature of 600 °C. The cone and collision gas (argon) flows were set to 20/25 l/h and 0.25/0.25 ml/min, respectively. The source temperature remained at 150 °C.

Chromatographic data were analyzed with Waters MassLynx v4.1 software. Quantification was achieved for each analyte using linear regression analysis of the peak area ratio analyte/IS (weighed 1/×) versus concentration. The assay

was performed for technical triplicates of cell lysates and data were corrected for total protein concentration.

Glycerol 3-phosphate

Quantification of glycerol 3-phosphate in DBS and cell lysates was performed on a Thermo Q-Exactive HF liquid chromatography system (Thermo Scientific, Bremen, Germany).

Samples were prepared by taking a 3-mm punch from each DBS and adding 500-µl methanol absolute ULC/MS (Biosolve BV, Valkenswaard, The Netherlands), followed by a 20-minute ultrasonication step. For cell lysates from HEK293 cells, 500-µl of samples was used.

Calibration standards were prepared with internal standards in the concentration range of 0.24–290 µM. 20 µl of $^{13}C_3$-Lactate internal standard (1 mM) was added to 500-µl methanol sample extract or 50-µl standard dilutions. Next, the samples were evaporated under a gentle flow of nitrogen at 40 °C and reconstituted in 30% Methanol/Milli-Q water.

Chromatographic separation was performed on a Dionex ultimate 3000 quaternary UHPLC (Thermo Scientific, Germering, Germany) equipped with a refrigerated autosampler (15 °C) and a column heater (55 °C) using an Synergi Hydro-RP 80A column (250 mm × 2 mm i.d., 4 µm; Phenomenex (Macclesfield, Cheshire, UK).

The following eluents were used: solvent A contained 10% methanol (v/v) and 750 mg/l octylammonium acetate (w/v) dissolved in water provided by a Millipore system; solvent B contained 90% methanol (v/v) and 750 mg/l octylammonium acetate (w/v). The gradient elution was as follows: 0–7.0 min isocratic 20% B, 7.0–8.5 min linear from 20 to 100% B, 8.5–11.5 min isocratic 100% B, and 11.5–12.0 linear from 100 to 20% B, with 12.0–15 min for initial conditions of 20% B for column equilibration. The flow rate remained constant at 0.5 ml/min. Injection volume was 5 µl.

The octylammonium acetate was made by dissolving 0.1 mol of octylamine (12.9 g) and 0.1 mol of concentrated acetic acid (6 g) in 100 ml of diethyl ether on ethanol/dry ice bath. The cooled solution was constantly mixed with a magnetic stirrer. After the octylammonium acetate salt crystallized, the ether was removed and the solid crystals were washed twice with 50 ml of n-hexane. Before preparation of the HPLC eluents, the octylammonium acetate was frozen at − 20 °C. Sodium L-lactate-$^{13}C_3$ solution 45–55% (w/w) in H_2O, octylamine, and L-Glycerol-3-phosphate lithium salt were purchased from Sigma-Aldrich. Acetic acid (> 99% purity) was purchased from Merck, Sharpe & Dohme BV.

Detection of glycerol 3-phosphate was performed using a Q-Exactive HF mass spectrophotometer (Thermo Scientific, Bremen, Germany) with an ESI source operating in full scan negative ionisation mode. Parameters for ESI–MS analysis in negative ion mode were as follows: scan range 70–600 *m/z* with a resolution of 120,000, AGC target 1e6, maximum IT 200 ms, capillary voltage 4 kV, capillary temperature 300 °C, sheath gas 50, aux gas 20, sweep gas 0, S-lens RF level 65. Quantification *m/z* for the compounds measured in the negative ion mode was as follows: $^{13}C_3$-lactate: 92.03448 *m/z*, Glycerol-3-phosphate: 171.0064 *m/z*. Data were acquired and processed using Thermo Scientific Xcalibur v 4.1.31.9 and Tracefinder v.4.1. The assay was performed for technical triplicates of cell lysates and data were corrected for total protein concentration.

Direct-infusion-based metabolomics

A non-quantitative direct-infusion high-resolution mass spectrometry metabolomics method was used as previously described (Haijes et al. 2019). In brief, dried blood spots (DBS) from 30 different Dutch controls, 3 Saudi Arabic Controls and both patients were measured in a single batch. A 3-mm punch from each DBS was made and 140-µl working solution was added, followed by a 20-min ultrasonication step. For cell lysates from HEK293 cells, 70-µl cell working solution was added to 70 µl of cell lysate in methanol. Both DBS and cell lysate samples were diluted with 60 µl 0.3% formic acid (Emsure, Darmstadt, Germany). Next, the solutions were filtered using a methanol preconditioned 96-well filter plate (Acro prep, 0.2-um GHP, NTRL, 1-ml well; Pall Corporation, Ann Arbor, MI, USA) and a vacuum manifold. The sample filtrate was collected in a 96-well plate (Advion, Ithaca, NY, USA).

Samples were analyzed using a TriVersa NanoMate system (Advion, Ithaca, NY, USA) controlled by Chipsoft software (version 8.3.3, Advion). Data acquisition was performed using Xcalibur software (version 3.0, Thermo Scientific, Waltham, MA, USA). A peak calling pipeline, developed in R programming language, annotated the raw mass spectrometry data according to the Human Metabolome DataBase (HMDB).

For each annotated mass peak in the DBS samples, the deviation of the intensities of the sample of interest compared to the control samples was indicated by a *Z*-score. This *Z*-score was calculated by: *Z*-score = (intensity patient sample − mean intensity control samples/standard deviation intensity control samples. Next, metabolites were identified as increased when Saudi Arabic controls had a *Z*-score below 2.5 and patients had *Z*-scores above 2.5. The list of increased metabolites is displayed in supplemental Table 1, sorted from highest to lowest mean *Z*-score.

Results

Clinical history

Index patient 1 is a 25-month-old Saudi boy. He was born prematurely at 32 weeks following an uneventful pregnancy.

He spent 3 weeks in the NICU mainly for weight management, during which he required a blood transfusion. At age 13 months, the pediatrician noted a global developmental delay and progressive microcephaly (OFC was 35.5 cm at 3 m of age, −3.6 SD). He was able to roll over but not to sit or crawl and his babbling was minimal. There was episodic up-rolling of the eyes suggestive of seizures. At 14 months of age, physical examination revealed microcephaly (OFC 41.5 cm, −4.6 SD), poor growth with length of 70 cm (−2.7 SD) and weight of 8.75 kg (3rd centile), dysmorphic facies (tall forehead, depressed nasal bridge, prominent infraorbital creases, long philtrum, open mouth and everted lower lip), axial hypotonia and hypertonia of the extremities with hyperactive reflexes. EEG revealed a hypsarrhythmia pattern confirming the clinical suspicion of epilepsy. MRI brain showed partial agenesis of predominately the splenium of the corpus callosum, prominent ventricles, and mild hypoplasia of the inferior vermis and pons. He was started on antiepileptic medications with only partial response. His healthy consanguineous parents (Fig. 2a for pedigree) had experienced recurrent miscarriages. His 4-year-old female cousin (Fig. 2b) had a similar phenotype, with severe global developmental delay (walking at 3 years and a vocabulary of only a few words at 4 years of age), epilepsy (controlled with antiepileptic medication, Table 1), microcephaly (OFC 47 cm, −2 SD), and similar facial dysmorphisms (Fig. 2b). Her brain MRI showed mild shortening of the corpus callosum and a normal pons and ventricles. Chromosomal microarray and exome sequencing following the routine diagnostic pipeline did not yield a cause for the clinical phenotype, nor did plasma amino acid, acylcarnitine, lactate, and urine organic acid analysis in both patients.

WES results

We enrolled both individuals and their parents with informed consent under an IRB-approved research protocol (RAC# 2080006) to identify the underlying cause of their likely

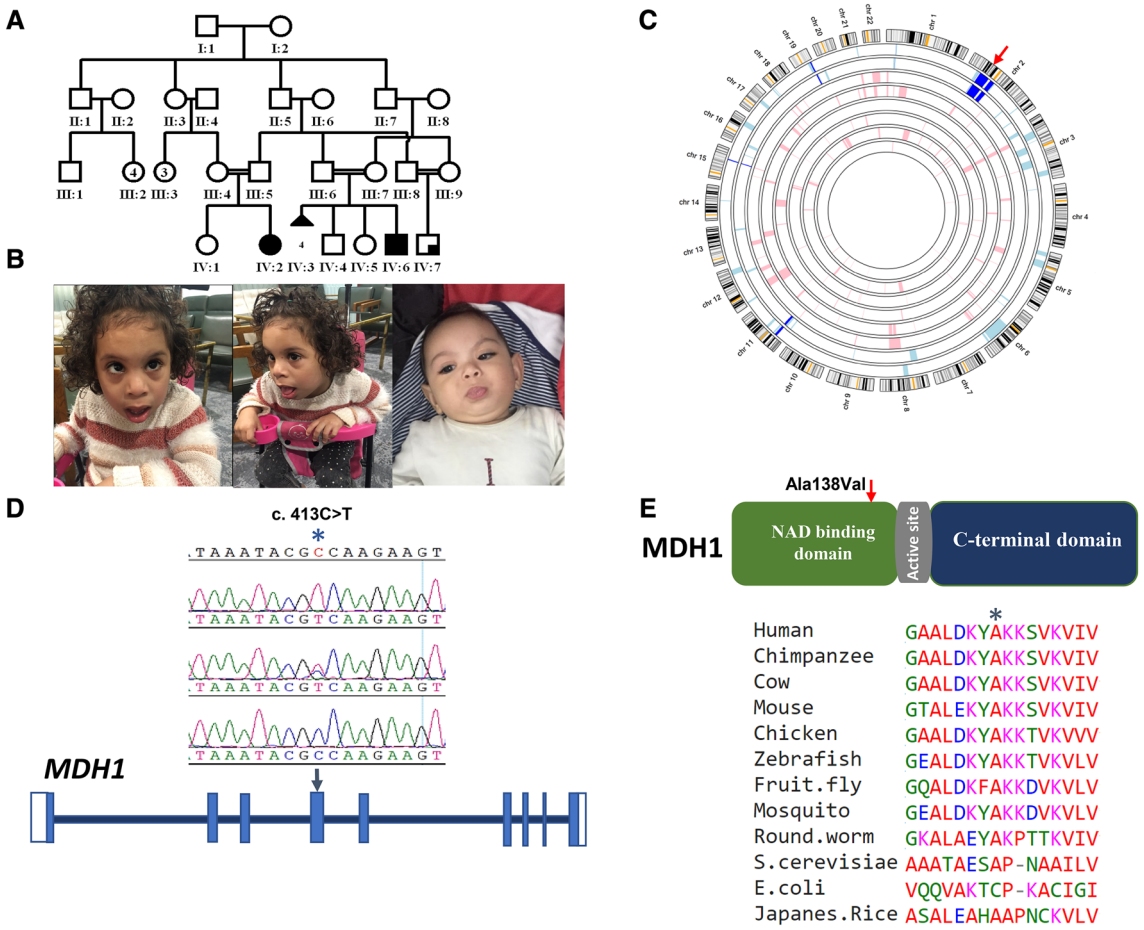

Fig. 2 **a** Pedigree of the affected family. **b** Clinical photographs of the two affected individuals. **c** Autozygome analysis using Agile mapper ideogram showing the candidate autozygome in dark blue. **d** Sequence chromatogram of the variant (top tracing corresponds to a homozygous patient, middle corresponds to a carrier and bottom corresponds to normal control) shown and its location on a cartoon of MDH1. **e** Degree of conservation of the affected amino acid residue

Table 1 Clinical presentation

	Clinical and genetic findings	
Origin	Saudi Arabia	Saudi Arabia
Family	Family-1	Family-1
Age	2.5 years	4 years
Sex	Male	Female
Consanguinity	Yes	Yes
ID on the pedigree	(IV:6)	(IV:2)
Genetic variant	MDH1:NM_001199111::c.413C > T:p.Ala138Val	MDH1:NM_001199111::c.413C > T:p.Ala138Val
Zygosity	Homozygous	Homozygous
NICU	Product of 32 week, birth weight 1.4 kg, admitted at NICU for 7 days, discharged home with 2 kg weight, 1 week later, re admitted with respiratory distress, found to have mild acidosis, had repeated visit to the hospital because of respiratory distress	No NICU admission
Growth parameters	OFC 41.5 cm (− 4.6 SD), length 70 cm (− 2.7 SD) and weight 8.75 kg (3rd centile),	OFC 47 cm (− 2 SD)
Age at which growth parameters were taken	14 m	4 years
Developmental history	Global developmental delay	Global developmental delay
Dysmorphic features	Microcephaly, plagiocephaly, bulbous nose, deep eyes, frontal bossing, micrognathia, strabismus	Microcephaly, plagiocephaly, bulbous nose, deep eyes, frontal bossing, micrognathia, strabismus
Ophthalmology	Normal retina	NA
Hematology	Normal CBC	Normal CBC
EEG	Consistent with epileptic encephalopathy, similar to hypsarrhythmic pattern	Normal
Brain MRI	Thinning and hypogenesis of the corpus callosum predominately the splenium. There is paucity of the white matter mainly in the posterior region with prominent peri-cerebral CSF spaces with asymmetry of the lateral ventricle predominantly prominent on the left side and posterior horn representing ex vacuo dilatation. There is mildly hypoplastic inferior vermis with mild pontine hypoplasia	Sagittal T1 revealed mild short corpus callosum, however, revealed normal signal intensity Axial T2 revealed mildly short corpus callosum, however, it shows normal signal intensity Axial T2 revealed normal myelination process which could be compatible with the age of the patient. 3D SPGR revealed no gross cortical abnormalities Normal configuration of the brainstem. The pituitary gland revealed normal size and signal intensity with no gross abnormality seen within hypothalamus region
Laboratory findings	Tandem MS urine GCMS, ammonia and lactate was within normal limits	Tmms: N, URO: N, lactate: 2.3, ammonia: N
Diagnosis	Severe progressive microcephaly, GDD and epilepsy	Severe developmental delay and microcephaly
Medications	Topamax 37.5 mg p.o. b.i.d and Clonazepam 0.1 mg p.o. b.i.d	

autosomal recessive condition. We performed autozygome analysis as described before (Alkuraya 2012) which revealed four autozygous intervals that were exclusively shared by the two affected individuals (Fig. 2c). We also proceeded with whole exome sequencing on the index patient and filtered the resulting variants by the coordinates of the candidate autozygome as described before (Alkuraya 2013). Only one homozygous variant was identified that was absent both in gnomAD and in a local database of ~2300 ethnically matched exomes: *MDH1*:NM_001199111:c.413C > T (Fig. 2d). The resulting missense variant p.Ala138Val replaces an absolutely conserved alanine (down to yeast and rice) in the NAD^+-binding domain (Fig. 2e). This variant segregated with the phenotype in a fully penetrant autosomal recessive fashion within the family.

MDH1 deficiency leads to aberrations in MAS-related metabolites

To study the potential pathogenicity of the *MDH1* variant, we assessed protein expression levels. MDH1 protein level was greatly reduced compared to controls in both lymphoblastoid cells (80%) and fibroblasts (70%) derived from both affected individuals (Fig. 3). We then aimed to identify the

metabolic consequences of MDH1 deficiency. To this end, MDH1 knockout HEK293 cells were generated by Crispr/Cas9 (Figure S1). Since the MAS plays an integral role in TCA and amino acid metabolism, compounds from both metabolic pathways were analyzed in dried bloodspots (DBS) and in MDH1 knockout cells. Targeted LC–MS/MS analysis revealed high concentrations of glutamate and a decreased glutamine/glutamate ratio compared to controls (Fig. 4a, b) in DBS, but not in the KO cell lysates (Figures S2 and S3). In addition, analysis of MDH1 KO cell lysates revealed an increase in aspartate and a decrease in fumarate levels (Fig. 4c, d), findings that were not observed in DBS (data not shown). No clear differences were found in concentrations of other TCA cycle intermediates, with the exception of low malate levels in one of the KO cell lysates (Figures S4 and S5).

Untargeted metabolomics reveals increased levels of glycerol 3-phosphate

To map additional biochemical consequences of MDH1 deficiency, we performed untargeted metabolomics in both DBS and MDH1 knockout HEK293 cells using direct-infusion mass spectrometry. Untargeted metabolomics revealed increased concentrations of a metabolite corresponding in mass with glycerol 3-phosphate (glycerol-3-*P*) in DBS of both individuals compared to controls (Fig. 5a). All other metabolites with *Z*-scores above 2.5 are listed in supplemental Table 1. Similarly, increased levels of glycerol-3-*P* were found in MDH1 KO HEK293 cells when compared to controls (Fig. 5b). However, since direct-infusion mass spectrometry does not distinguish between isomers, the identification of glycerol 3-*P* is limited, as beta-glycerophosphoric acid (glycerol 2-*P*) has the same mass. To this end, these findings were validated using targeted measurements

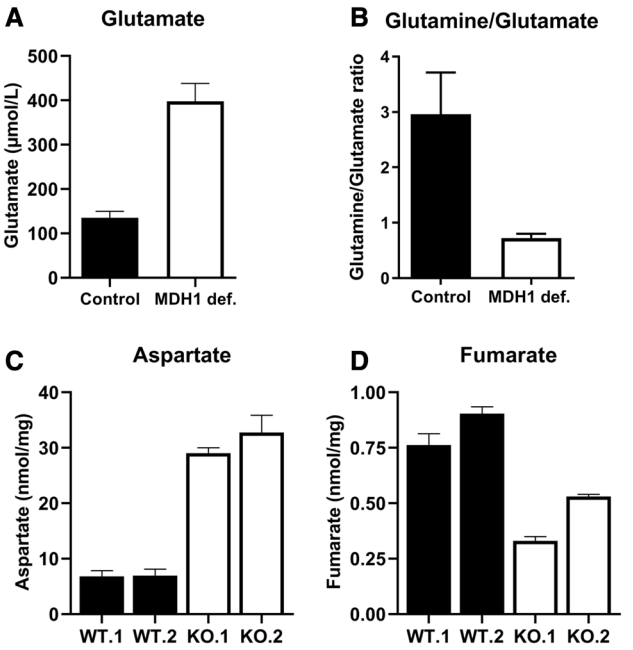

Fig. 4 MDH1 deficiency leads to aberrations in MAS-related metabolites. **a** Glutamate concentration and **b** Glutamine/Glutamate ratio in dried bloodspots (control $n=3$, MDH1 def. $n=2$). Data are presented as mean ± SD. **c** Aspartate and **d** fumarate concentrations in *MDH1* HEK293 cells (WT $n=2$, KO $n=2$). Data are presented as mean ± SD for technical triplicates

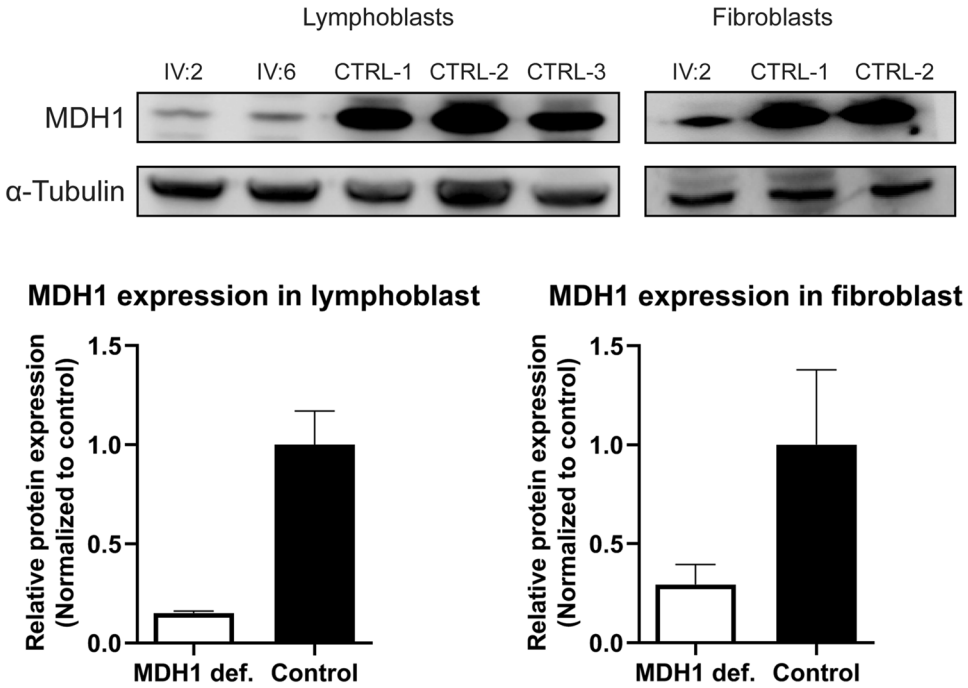

Fig. 3 Western blot analysis of MDH1 in protein extracts from LCL as well as fibroblast cells from the affected individuals compared to controls. Relative MDH1 expression is shown as mean ± SD for both patients and controls 1 and 3 in lymphoblasts. For fibroblasts, relative expression is shown as mean ± SD for technical triplicates of the patient, and individual data points for both controls

of glycerol 3-*P*. In DBS of both individuals high concentrations of glycerol 3-*P* were found compared to control (Fig. 5c), but in cell lysates, the difference between MDH1 KO and controls was no longer significant (Fig. 5d).

Discussion

We report a family with a neurodevelopmental disorder characterized by global developmental delay, epilepsy and progressive microcephaly and a homozygous MDH1 candidate causal variant. This neurological phenotype highly resembles the phenotype that was observed in patients with MDH2 and other MAS deficiencies and might, thus, well represent the clinical consequences of this group of disorders. A notable exception is that we did not find lactic acidemia in our patients. Since MDH1 and MDH2 are localized into different subcellular compartments, this is not surprising. Lactic acidemia is often a characteristic of mitochondrial dysfunction, caused by compensatory ATP production via glycolysis (McInnes 2013). Lactic acidemia is expected in MDH2 deficiency given its role linked to the mitochondrial electron transport chain (Ait-El-Mkadem et al. 2017), but might not be seen in MDH1 deficiency because of hampered glycolysis.

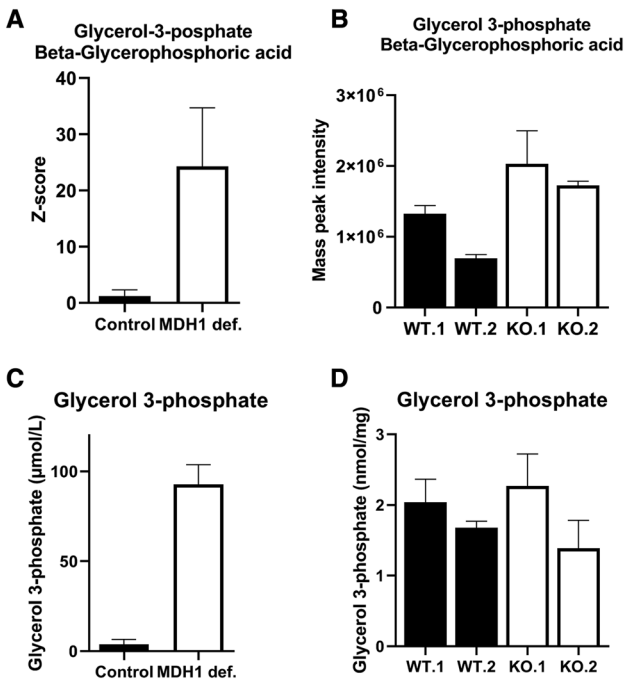

Fig. 5 Untargeted metabolomics revealed increased levels of glycerol 3-phosphate. **a** *Z*-scores annotated for glycerol 3-phosphate and beta-glycerophosphoric acid in dried blood spots (control $n=3$; MDH1 def. $n=2$). **b** Raw mass peak intensities annotated for glycerol 3-phosphate and beta-glycerophosphoric acid in *MDH1* HEK293 cells. **c** Glycerol 3-phosphate concentration in dried blood spots (control $n=3$; MDH1 def. $n=2$) and **d** *MDH1* HEK293 cells. Data from *MDH1* HEK293 cells are presented as mean ± SD for technical triplicates

The mechanism of how MDH1 deficiency may cause the observed neurodevelopmental phenotype is unclear. Both children presented with global developmental delay, progressive microcephaly, epilepsy, axial hypotonia and hypertonia of the extremities. The combination of these clinical symptoms suggests underlying problems in the central nervous system. This is further supported by the abnormal findings on neuroimaging and would be consistent with the important role of the MAS in neurons (McKenna et al. 2006).

One of the biochemical findings in dried blood spots (DBS) of both patients was the elevated level of glutamate. In addition, increased levels of a bile acid (3-oxo-4,6-choladienoic acid, Table S1) were found. Since primary functions of the liver include breakdown of amino acids and the production and excretion of bile acids, these findings might indicate subclinical liver problems in the patients. The regulation of MAS enzymes and transporters also has an important influence on glutamate metabolism in the brain (McKenna et al. 2006; Gruetter et al. 2003; Malik et al. 1993). Although glutamate cannot cross the blood–brain barrier, the increased glutamate levels in the blood may reflect similar metabolic consequences as in the brain. Glutamate acts as an important excitatory neurotransmitter in the brain (McKenna 2007). Neurons are able to synthesize glutamate from its local precursor a-ketoglutarate via GOT1, using aspartate as nitrogen source (Palaiologos et al. 1988) (Pardo et al. 2011). The supply of cytosolic a-ketoglutarate for this transamination reaction occurs via the malate–oxoglutarate carrier, which exchanges cytosolic malate for mitochondrial a-ketoglutarate. However, to drive this exchange, sufficient cytosolic malate is required. A deficiency in MDH1 might decrease cytosolic malate availability. In addition, glutamate homeostasis may be affected in these cells. Disturbances in glutamate homeostasis are also seen in patients with epilepsy, in which a rise in extracellular glutamate levels has been observed (During and Spencer 1993; Cavus et al. 2005). Since both children presented with clinical symptoms of epilepsy, the increased glutamate levels in dried blood spots of the patients may be associated with the neurological clinical phenotype of MDH1 deficiency.

In contrast, no clear differences of glutamate concentration were found in our MDH1 KO HEK cell model compared to control. This is probably due to the fact that cell culture simply reflects metabolites from a single cell type, whereas dried blood spots reflect metabolites from multiple tissues.

Further analysis of the MDH1 KO cells identified two interesting phenomena: increased aspartate levels and decreased fumarate levels. Aspartate is essential for protein synthesis as well as for purine and pyrimidine biosynthesis

(Lane and Fan 2015). Increased levels of aspartate were also previously identified in a MDH1 KO model of Jurkat cells (Birsoy et al. 2015). Transamination of aspartate to oxaloacetate by GOT1 has been shown to support generation of malate via MDH1 (Gaude et al. 2018). In MDH1 deficiency, oxaloacetate cannot be converted into malate, which may result in accumulation of its precursor aspartate. The decreased levels of fumarate in MDH1 KO cells might also indicate a disruption in several pathways. Cytosolic fumarate is transported into mitochondria to be recycled for cytosolic aspartate via the TCA cycle and MAS enzymes and transporters. A defect in recycling cytosolic aspartate, which is a precursor for malate in the MAS, might be compensated via increased conversion of fumarate into malate. Cytosolic malate has been shown to be essential for the transport of glutamate into mitochondria via the AGC (Rasmussen and Rasmussen 2000), since malate is also a precursor of mitochondrial aspartate via oxaloacetate. In addition, transport of malate in mitochondria is important for pyruvate oxidation and feeding in the TCA cycle. The identified metabolic consequences of MDH1 deficiency involve metabolites that are directly linked to both substrates of MDH1. However, since transporters and enzymes of the MAS, TCA and also the urea cycle share overlapping metabolic mechanisms involving MDH1, these biochemical aberrations may reflect a more complex mechanism. Future work regarding functional pathway analysis is required to elucidate the exact role of these metabolites in MDH1 deficiency.

Using untargeted metabolomics, we were able to discover a potential biomarker for this new deficiency. Increased levels of glycerol 3-phosphate (glycerol-3-*P*) were revealed in DBS of both patients compared to controls. The accumulation of glycerol-3-*P* may be a logical consequence of MDH1 deficiency. Glycerol-3-*P* is an oxidative product of the cytosolic NADH-dependent glycerol-3-phosphate dehydrogenase (GPDH) and is part of the glycerol-phosphate (glycerol-*P*) shuttle (Fig. 1). This shuttle functions similarly to the MAS to mediate the cytosolic oxidation of NADH, but is mainly involved in triglyceride synthesis via regulation of cytosolic glycerol-3-*P* availability (Mráček et al. 2013). The glycerol-*P* shuttle has a variable expression over tissues, with highest expression in brown adipose tissue (Ohkawa et al. 1969). There is also evidence of glycerol-*P* shuttle activity in the central nervous system, with probably a more dominant role for the glycerol-*P* shuttle in astrocytes than in neurons (Nguyen et al. 2003; Ramos et al. 2003; McKenna et al. 1993). Increased levels of glycerol 3-*P* may be caused by increased GPDH activity due to high cytosolic NADH levels, which may partly compensate the consequences of MDH1 deficiency.

In conclusion, we propose that MDH1 deficiency is a new defect in the MAS causing a neurological phenotype. The elevated concentrations of glycerol-3-*P* in DBS of both patients suggest a potential role for glycerol 3-*P* as a biomarker in this novel metabolic disorder.

Acknowledgements We thank the patients and families for their enthusiastic participation. We also thank the Genotyping and Sequencing Core Facilities at KFSHRC for their technical help. We also thank Marjolein Bosma, Birgit Schiebergen-Bronckhorst, Johan Gerrits and Yuen Fung Tang for their technical assistance. This work was supported by King Salman Center for Disability Research (85721 to FSA); and Metakids (2017-075 to JJMJ).

Compliance with ethical standards

Conflict of interest Authors declare no conflict of interest.

References

Ait-El-Mkadem S, Dayem-Quere M, Gusic M, Chaussenot A, Bannwarth S, François B, Genin EC, Fragaki K, Volker-Touw CLM, Vasnier C et al (2017) Mutations in MDH2, encoding a krebs cycle enzyme, cause early-onset severe encephalopathy. Am J Hum Genet 100:151–159

Alkuraya FS (2012) Discovery of rare homozygous mutations from studies of consanguineous pedigrees. Curr Protoc Hum Genet 75:6.12.1–6.12.13

Alkuraya FS (2013) The application of next-generation sequencing in the autozygosity mapping of human recessive diseases. Hum Genet 132:1197–1211

Birktoft JJ, Fu Z, Carnahan GE, Rhodes G, Roderick SL, Banaszak LJ (1989) Comparison of the molecular structures of cytoplasmic and mitochondrial malate dehydrogenase. Biochem Soc Trans 17:301–304

Birsoy K, Wang T, Chen WW, Freinkman E, Abu-Remaileh M, Sabatini DM (2015) An essential role of the mitochondrial electron transport chain in cell proliferation is to enable aspartate synthesis. Cell 162:540–551

Cavus I, Kasoff WS, Cassaday MP, Jacob R, Gueorguieva R, Sherwin RS, Krystal JH, Spencer DD, Abi-Saab WM (2005) Extracellular metabolites in the cortex and hippocampus of epileptic patients. Ann Neurol 57:226–235

During MJ, Spencer DD (1993) Extracellular hippocampal glutamate and spontaneous seizure in the conscious human brain. Lancet 341:1607–1610

Falk MJ, Li D, Gai X, McCormick E, Place E, Lasorsa FM, Otieno FG, Hou C, Kim CE, Abdel-Magid N et al (2014) AGC1 deficiency causes infantile epilepsy, abnormal myelination, and reduced *N*-acetylaspartate. JIMD Rep 14:77–85

Gaude E, Schmidt C, Gammage PA, Dugourd A, Blacker T, Chew SP, Saez-Rodriguez J, O'Neill JS, Szabadkai G, Minczuk M et al (2018) NADH shuttling couples cytosolic reductive carboxylation of glutamine with glycolysis in cells with mitochondrial dysfunction. Mol Cell 69:581.e7–593.e7

Gruetter R, Adriany G, Choi I-Y, Henry P-G, Lei H, Öz G (2003) Localizedin vivo13C NMR spectroscopy of the brain. NMR Biomed 16:313–338

Haijes HA, Willemsen M, Van der Ham M, Gerrits J, Pras-Raves ML, Prinsen HCMT, Van Hasselt PM, Sain-van De, der Velden MGM, Verhoeven-Duif NM, Jans JJM (2019) Direct infusion based metabolomics identifies metabolic disease in patients' dried blood spots and plasma. Metabolites 9:12

Hanse EA, Ruan C, Kachman M, Wang D, Lowman XH, Kelekar A (2017) Cytosolic malate dehydrogenase activity helps support

glycolysis in actively proliferating cells and cancer. Oncogene 36:3915–3924
Joh T, Takeshima H, Tsuzuki T, Setoyama C, Shimada K, Tanase S, Kuramitsu S, Kagamiyama H, Morino Y (1987) Cloning and sequence analysis of cDNAs encoding mammalian cytosolic malate dehydrogenase. Comparison of the amino acid sequences of mammalian and bacterial malate dehydrogenase. J Biol Chem 262:15127–15131
Lane AN, Fan TW-M (2015) Regulation of mammalian nucleotide metabolism and biosynthesis. Nucleic Acids Res 43:2466–2485
Lee SM, Kim JH, Cho EJ, Youn HD (2009) A nucleocytoplasmic malate dehydrogenase regulates p53 transcriptional activity in response to metabolic stress. Cell Death Differ 16:738–748
Lee S-M, Dho SH, Ju S-K, Maeng J-S, Kim J-Y, Kwon K-S (2012) Cytosolic malate dehydrogenase regulates senescence in human fibroblasts. Biogerontology 13:525–536
Lo AS-Y, Liew C-T, Ngai S-M, Tsui SK-W, Fung K-P, Lee C-Y, Waye MM-Y (2005) Developmental regulation and cellular distribution of human cytosolic malate dehydrogenase (MDH1). J Cell Biochem 94:763–773
Malik P, McKenna MC, Tildon JT (1993) Regulation of malate dehydrogenases from neonatal, adolescent, and mature rat brain. Neurochem Res 18:247–257
McInnes J (2013) Mitochondrial-associated metabolic disorders: foundations, pathologies and recent progress. Nutr Metab (Lond) 10:63
McKenna MC (2007) The glutamate-glutamine cycle is not stoichiometric: fates of glutamate in brain. J Neurosci Res 85:3347–3358
McKenna MC, Tildon JT, Stevenson JH, Boatright R, Huang S (1993) Regulation of energy metabolism in synaptic terminals and cultured rat brain astrocytes: differences revealed using aminooxyacetate. Dev Neurosci 15:320–329
McKenna MC, Waagepetersen HS, Schousboe A, Sonnewald U (2006) Neuronal and astrocytic shuttle mechanisms for cytosolic-mitochondrial transfer of reducing equivalents: current evidence and pharmacological tools. Biochem Pharmacol 71:399–407
Mráček T, Drahota Z, Houštěk J (2013) The function and the role of the mitochondrial glycerol-3-phosphate dehydrogenase in mammalian tissues. Biochim Biophys Acta Bioenergy 1827:401–410
Nguyen NHT, Bråthe A, Hassel B (2003) Neuronal uptake and metabolism of glycerol and the neuronal expression of mitochondrial glycerol-3-phosphate dehydrogenase. J Neurochem 85:831–842
Ohkawa KI, Vogt MT, Farber E (1969) Unusually high mitochondrial alpha glycerophosphate dehydrogenase activity in rat brown adipose tissue. J Cell Biol 41:441–449
Olguín-Albuerne M, Morán J (2018) Redox signaling mechanisms in nervous system development. Antioxid Redox Signal 28:1603–1625
Palaiologos G, Hertz L, Schousboe A (1988) Evidence that aspartate aminotransferase activity and ketodicarboxylate carrier function are essential for biosynthesis of transmitter glutamate. J Neurochem 51:317–320
Palmieri L, Pardo B, Lasorsa FM, del Arco A, Kobayashi K, Iijima M, Runswick MJ, Walker JE, Saheki T, Satrústegui J et al (2001) Citrin and aralar1 are Ca^{2+}-stimulated aspartate/glutamate transporters in mitochondria. EMBO J 20:5060–5069
Pardo B, Rodrigues TB, Contreras L, Garzón M, Llorente-Folch I, Kobayashi K, Saheki T, Cerdan S, Satrústegui J (2011) Brain glutamine synthesis requires neuronal-born aspartate as amino donor for glial glutamate formation. J Cereb Blood Flow Metab 31:90–101
Prinsen HCMT, Schiebergen-Bronkhorst BGM, Roeleveld MW, Jans JJM, de Sain-van der Velden MGM, Visser G, van Hasselt PM, Verhoeven-Duif NM (2016) Rapid quantification of underivatized amino acids in plasma by hydrophilic interaction liquid chromatography (HILIC) coupled with tandem mass-spectrometry. J Inherit Metab Dis 39:651–660
Ramos M, del Arco A, Pardo B, Martínez-Serrano A, Martínez-Morales JR, Kobayashi K, Yasuda T, Bogónez E, Bovolenta P, Saheki T et al (2003) Developmental changes in the Ca^{2+}-regulated mitochondrial aspartate-glutamate carrier aralar1 in brain and prominent expression in the spinal cord. Brain Res Dev Brain Res 143:33–46
Rasmussen UF, Rasmussen HN (2000) Human quadricepts muscle mitochondria: a functional characterization. Mol Cell Biochem 208:37–44
Saheki T, Kobayashi K (2002) Mitochondrial aspartate glutamate carrier (citrin) deficiency as the cause of adult-onset type II citrullinemia (CTLN2) and idiopathic neonatal hepatitis (NICCD). J Hum Genet 47:333–341
Song Y-Z, Deng M, Chen F-P, Wen F, Guo L, Cao S-L, Gong J, Xu H, Jiang G-Y, Zhong L et al (2011) Genotypic and phenotypic features of citrin deficiency: five-year experience in a Chinese pediatric center. Int J Mol Med 28:33–40
Tanaka T, Inazawa J, Nakamura Y (1996) Molecular cloning and mapping of a human cDNA for cytosolic malate dehydrogenase (MDH1). Genomics 32:128–130
van Karnebeek CDM, Ramos RJ, Wen X-Y, Tarailo-Graovac M, Gleeson JG, Skrypnyk C, Brand-Arzamendi K, Karbassi F, Issa MY, van der Lee R et al (2019) Bi-allelic GOT2 mutations cause a treatable malate-aspartate shuttle-related encephalopathy. Am J Hum Genet 105(3):534–548. https://doi.org/10.1016/j.ajhg.2019.07.015
Webb LE, Hill EJ, Banaszak LJ (1973) Conformation of nicotinamide adenine dinucleotide bound to cytoplasmic malate dehydrogenase. Biochemistry 12:5101–5109
Wibom R, Lasorsa FM, Töhönen V, Barbaro M, Sterky FH, Kucinski T, Naess K, Jonsson M, Pierri CL, Palmieri F et al (2009) AGC1 deficiency associated with global cerebral hypomyelination. N Engl J Med 361:489–495
Zhang B, Tornmalm J, Widengren J, Vakifahmetoglu-Norberg H, Norberg E (2017) Characterization of the role of the malate dehydrogenases to lung tumor cell survival. J Cancer 8:2088–2096